Supplementary Information

Local Structural Distortion of $BaZr_xTi_{1-x}O_3$ Nanocrystals Synthesized at Room Temperature

Federico A. Rabuffetti and Richard L. Brutchey

Department of Chemistry, University of Southern California, Los Angeles, CA 90089, USA

Experimental

Synthesis. *General procedures.* All manipulations were conducted at room temperature under N_2 atmosphere using standard Schlenk techniques.

Reagents. Ba–Zr and Ba–Ti double metal alkoxide solutions from Gelest Inc. were employed as precursors for the synthesis of $BaZr_xTi_{1-x}O_3$ nanocrystals. The nominal molarities of the heterometallic precursor solutions were 0.33 and 0.50 M for Ba–Zr and Ba–Ti, respectively.

Apparatus. The apparatus employed for the synthesis $BaZr_xTi_{1-x}O_3$ nanocrystals via vapor diffusion is shown in Fig. S1. It consists of a 100-mL three-neck flask featuring two gas adapters (A and B) with glass stopcocks; the first connects the reaction flask to the N_2 gas line and the second acts as a vent. In addition, the system features a glass bubbler filled with 50 mL of a 0.75 M HCl solution; the inlet of the bubbler is connected to a needle-valve rotameter, which is in turn connected to the N_2 gas line. The outlet of the bubbler is connected via tygon tubing to a third gas adapter (C) featuring a glass stopcock; this gas adapter allows connection of the bubbler to the reaction flask. The system has two operating configurations: (1) precursor injection (not shown in Fig. S1), in which stopcock A is open, B is closed, and a suba septum replaces C, and (2) vapor diffusion, in which stopcock A is closed, and B and C are open, thereby allowing N_2 gas saturated in HCl/H_2O vapor to flow over the precursor solution. The vapor flow rate can be controlled via the needle-valve rotameter.

Synthesis of $BaZr_xTi_{1-x}O_3$ nanocrystals. At the beginning of the each synthetic procedure, the system was set for precursor injection (A open, B closed, and a suba septum replacing C). Then, for each $BaZr_xTi_{1-x}O_3$ composition, the corresponding volume of each heterometallic precursor was transferred via syringe to the 100-mL three-neck flask to give a total volume of 2.0 mL. For example, in the case of $BaZr_{0.4}Ti_{0.6}O_3$, 1.0 mL (0.33 mmol) of the Ba−Zr precursor and 1.0 mL (0.50 mmol) of the Ba−Ti precursor were mixed in the reaction flask. Simultaneously, N_2 was bubbled through the 0.75 M HCl solution. After 30 min of vigorous bubbling, the bubbler was connected to the reaction flask by quickly replacing the suba septum with gas adapter C and the system configuration was switched to vapor diffusion (A closed, and B and C open). An increase in the viscosity of the solution was observed upon continuous flow of $N_2/HCl/H_2O$ vapor. This was observed to happen first near the walls of reaction flask, and then move radially inward. After a certain time, this resulted in the formation of a fully rigid, monolithic, and crack-free gel. For $BaZr_xTi_{1-x}O_3$ nanocrystals synthesized in this work, the N_2 flow rate was adjusted to obtain gelation times of ~5.5 h and maintained constant throughout the whole reaction time. A few hours after the formation of the monolithic gel, cracks started to appear. Simultaneously, the presence of a clear supernatant was observed; both the cracks and the amount of supernatant grew with time, yielding several small pieces of gel. No precipitation or turbidity was observed at any point of the process. After 72 h, the $N_2/HCl/H_2O$ vapor flow was stopped, the reaction flask opened, and pieces of the gel collected. These were washed with 5 mL of absolute ethanol, sonicated for 10 min, and centrifuged at 6000 rpm for 25 min; this washing step was repeated three times. The resulting particles were dried under vacuum at room temperature for 4 h, yielding a fine, off-white powder. In a typical synthesis, yields ranging from 70 to 80% were achieved. Identical synthesis conditions (temperature, gelation time, and total reaction time) and postsynthesis treatments (washing and drying) were employed for all $BaZr_xTi_{1-x}O_3$ compositions.

Characterization. ***Conventional powder X-ray diffraction.*** Conventional X-ray diffraction patterns of $BaZr_xTi_{1-x}O_3$ nanocrystals were collected in the 20–80° 2θ range using a Rigaku Ultima IV diffractometer operated at 44 mA and 40 kV. Cu Kα radiation (λ = 1.5406 Å) was employed. The step size and collection time were 0.025° and 1 s per step, respectively. Diffraction patterns were recorded at 25 °C.

Synchrotron powder X-ray diffraction. Synchrotron X-ray diffraction patterns were collected in the 3–40° 2θ range at the 11−BM line of the Advanced Photon Source of Argonne

National Laboratory. An incident photon energy of 30.062 keV (λ = 0.412432 Å) monochromated using a Si (111) double crystal was employed. Diffraction patterns were collected in transmission mode. The step size and scan speed were 0.001° and 0.01° s^{-1}, respectively. Diffraction patterns were recorded at 25 °C.

Rietveld analysis. Structural refinement was carried out by means of Rietveld[1,2] analysis of synchrotron X-ray diffraction data; the General Structure Analysis System (GSAS)[3] software suite was employed to that end. For each composition of the $BaZr_xTi_{1-x}O_3$ solid solution, two phases were refined: $BaZr_xTi_{1-x}O_3$ (cubic space group $Pm{-}3m$) with stoichiometry identical to the nominal composition, and $BaCO_3$ (orthorhombic space group $Pmcn$). This carbonate phase, which is not observed in the X-ray diffraction patterns of fresh samples, arises from the chemisorption of atmospheric CO_2 upon extended exposure of the nanocrystals to air. The following parameters were refined: (1) scale factor for each phase, (2) background, which was modeled using a shifted Chebyschev polynomial function, (3) peak shape for each phase, which was modeled using a modified Thomson–Cox–Hasting pseudo-Voight[4] function including an asymmetry parameter, (4) lattice parameters (i.e., a for the perovskite phase, and a, b, and c for the carbonate phase), and (5) isotropic temperature factors for each atom of the perovskite phase (i.e., U_{Ba}, $U_{\mathrm{Zr,Ti}}$, and U_{O}). Atomic scattering factors were corrected for anomalous scattering and, for each composition, experimental data were corrected for X-ray absorption by the corresponding perovskite phase. The usual R_F^2, R_{wp}, and χ^2 indicators were employed to assess the quality of the refined structural models.

Raman spectroscopy. Raman spectra were recorded under ambient conditions using a Nicolet Magna 850 FT-Raman. 1064 nm radiation from a Nd:YAG laser was employed as the excitation source and the power at the sample level was 300 mW. For each $BaZr_xTi_{1-x}O_3$ composition, 300 scans were collected using a spectral resolution of 8 cm^{-1}. Sulfur and 4-acetamidophenol were employed as frequency standards for calibration of Raman shifts. The absolute accuracy of Raman shifts was estimated to be ±1.5 cm^{-1}.

Transmission electron imaging (TEM). TEM images were obtained using a JEOL JEM2100F (JEOL Ltd.) electron microscope operated at 200 kV. Specimens for transmission electron microscopy studies were prepared using a two-step procedure. First, a tiny amount of sample was dispersed in methanol and sonicated for 30 min. Then, a drop of the resulting suspension was deposited on a 200 mesh Cu grid coated with a Lacey carbon film (Ted Pella Inc.).

Dielectric characterization. Pellets for preliminary dielectric studies were prepared by grinding ~200 mg of $BaZr_xTi_{1-x}O_3$ nanocrystals with 1 mL of a 1 mg mL^{-1} aqueous solution of polyvinyl alcohol. The resulting slurry was allowed to dry for 8 h under N_2 atmosphere. The dry powder was pressed into a 13 mm diameter pellet by applying ~4 metric tons of pressure for 3 mins in vacuo. Then, the pressed pellet was thermally treated at 150 °C for 2.5 h under N_2 flow. The resulting pellet had a thickness of ~0.45 mm. Colloidal silver paint (Ted Pella Inc.) was applied to both sides of the pellet to form a simple cylindrical capacitor. Finally, the pellet was thermally treated at 100 °C for 1 h under N_2 flow and subsequently stored under N_2. Capacitance was measured using an Agilent 4294A Impedance Analyzer (Agilent Technologies) at a fixed frequency of 1 kHz; all measurements were carried out at 25 °C under N_2 atmosphere. The dielectric constant (ε_r) of $BaZr_xTi_{1-x}O_3$ nanocrystals was then extracted using Bruggeman's effective medium approximation:[5]

$$\sum_{i=1}^{n} v_i \frac{\varepsilon_i - \varepsilon_{eff}}{\varepsilon_i + (n-1)\varepsilon_{eff}} = 0$$

The pellet with effective dielectric constant ε_{eff} was modeled as a triphasic composite of $BaZr_xTi_{1-x}O_3$, air, and polyvinyl alcohol (i.e., $n = 3$).[6] The geometric density of the pellet was measured in order to estimate the volume fraction of each component (v_i); values ranging from 55 to 65% of the theoretical density for the corresponding $BaZr_xTi_{1-x}O_3$ composition were obtained. The density of air, and the density and mass of polyvinyl alcohol employed during the processing step were taken as 1.2×10^{-3} g cm^{-3}, 1.2 g cm^{-3}, and 1×10^{-3} g, respectively. Finally, values of 1.00059 and 1.95 were employed for the dielectric constant of air and polyvinyl alcohol, respectively.

References

1. H. M. Rietveld, *Acta Crystallogr.*, 1967, **22**, 151.
2. H. M. Rietveld, *J. Appl. Crystallogr.*, 1969, **2**, 65.
3. A. C. Larson and R. B. Von Dreele, Los Alamos National Laboratory, 2000.
4. P. Thompson, D. E. Cox and J. M. Hastings, *J. Appl. Crystallog.*, 1987, **20**, 79.
5. W. R. Tinga, W. A. G. Voss and D. F. Bloossey, *J. Appl. Phys.*, 1973, **44**, 3897.

6. R. Z. Hou, P. Ferreira and P. M. Vilarinho, *Chem. Mater.*, 2009, **21**, 3536.

Figures and Tables

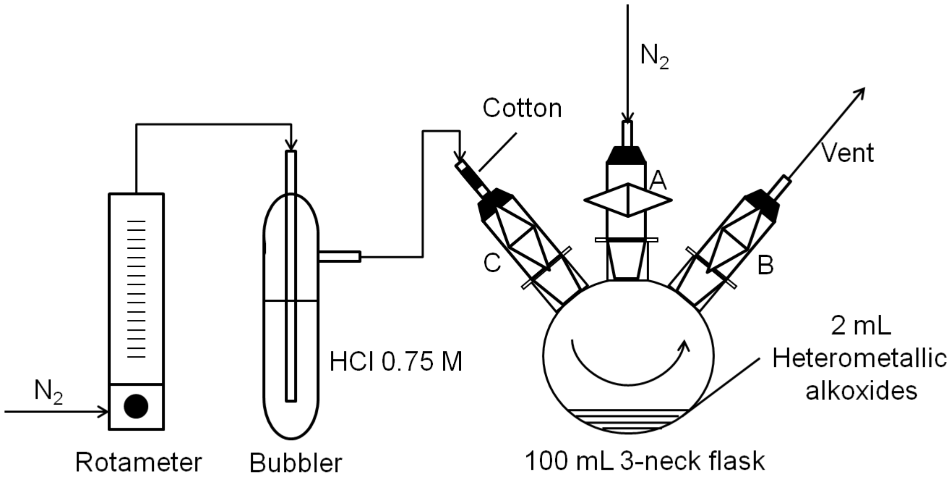

Fig. S1 Apparatus employed for the synthesis $BaZr_xTi_{1-x}O_3$ nanocrystals via vapor diffusion. The apparatus has two operating configurations: (1) precursor injection, in which A is open, B is closed, and a suba septum replaces C; and (2) vapor diffusion, in which stopcock A is closed, and B and C are open. The arrows depict the flow of N_2 gas through the system.

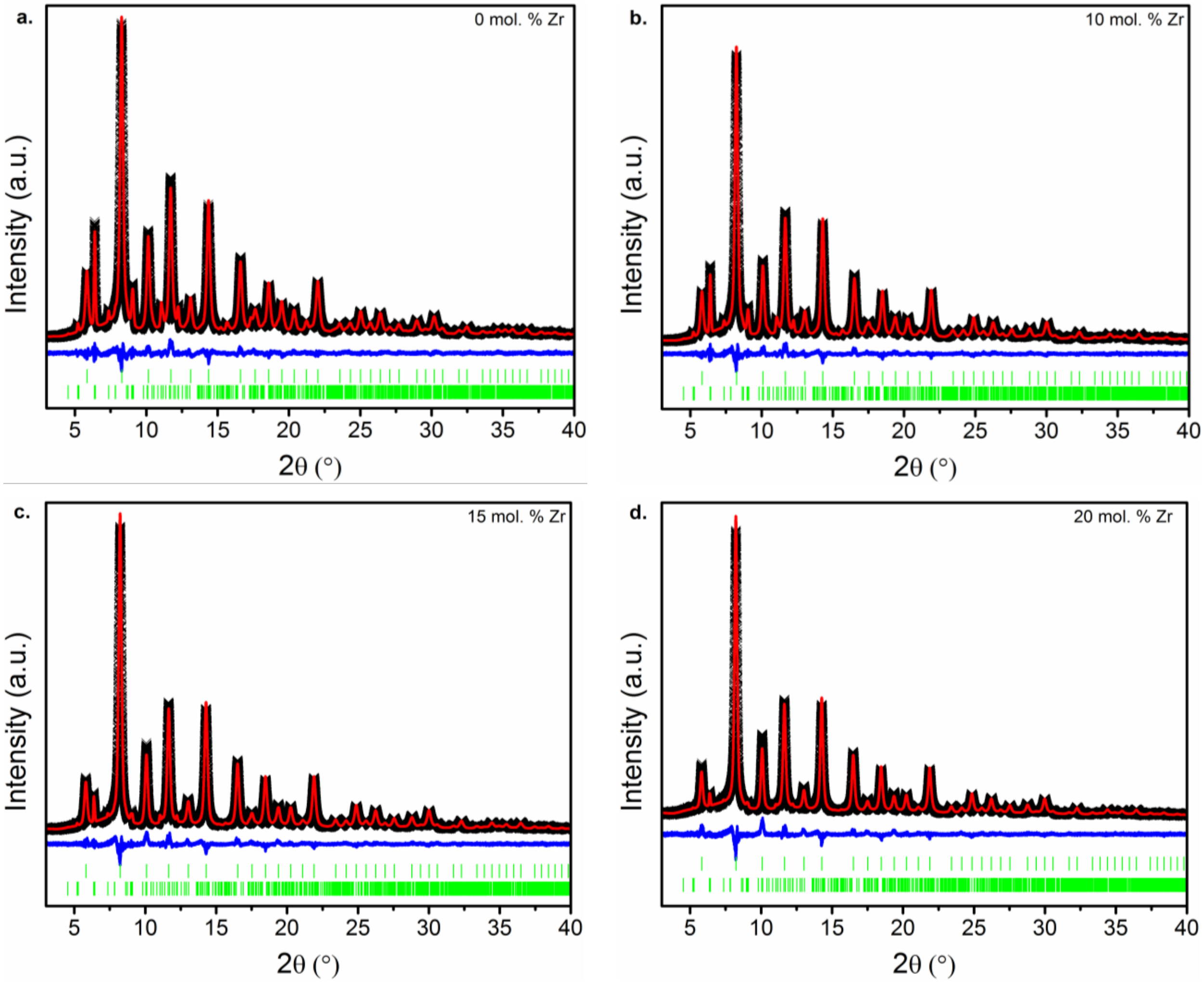

Fig. S2 Rietveld analyses of synchrotron X-ray diffraction patterns of BaZr$_x$Ti$_{1-x}$O$_3$ nanocrystals for the following compositions: (a) x = 0, (b) x = 0.1, (c) x = 0.15, and (d) x = 0.2. The experimental (×) and calculated (—) diffraction patterns are shown for each composition, along with the difference curve (—) and the thickmarks (|) corresponding to the two phases refined (upper thickmarks: cubic BaZr$_x$Ti$_{1-x}$O$_3$; lower thickmarks: orthorhombic BaCO$_3$). BaCO$_3$, which is not observed in the X-ray diffraction patterns of fresh samples, arises from the chemisorption of atmospheric CO$_2$ upon extended exposure of the nanocrystals to air.—*Continues on the following page*.

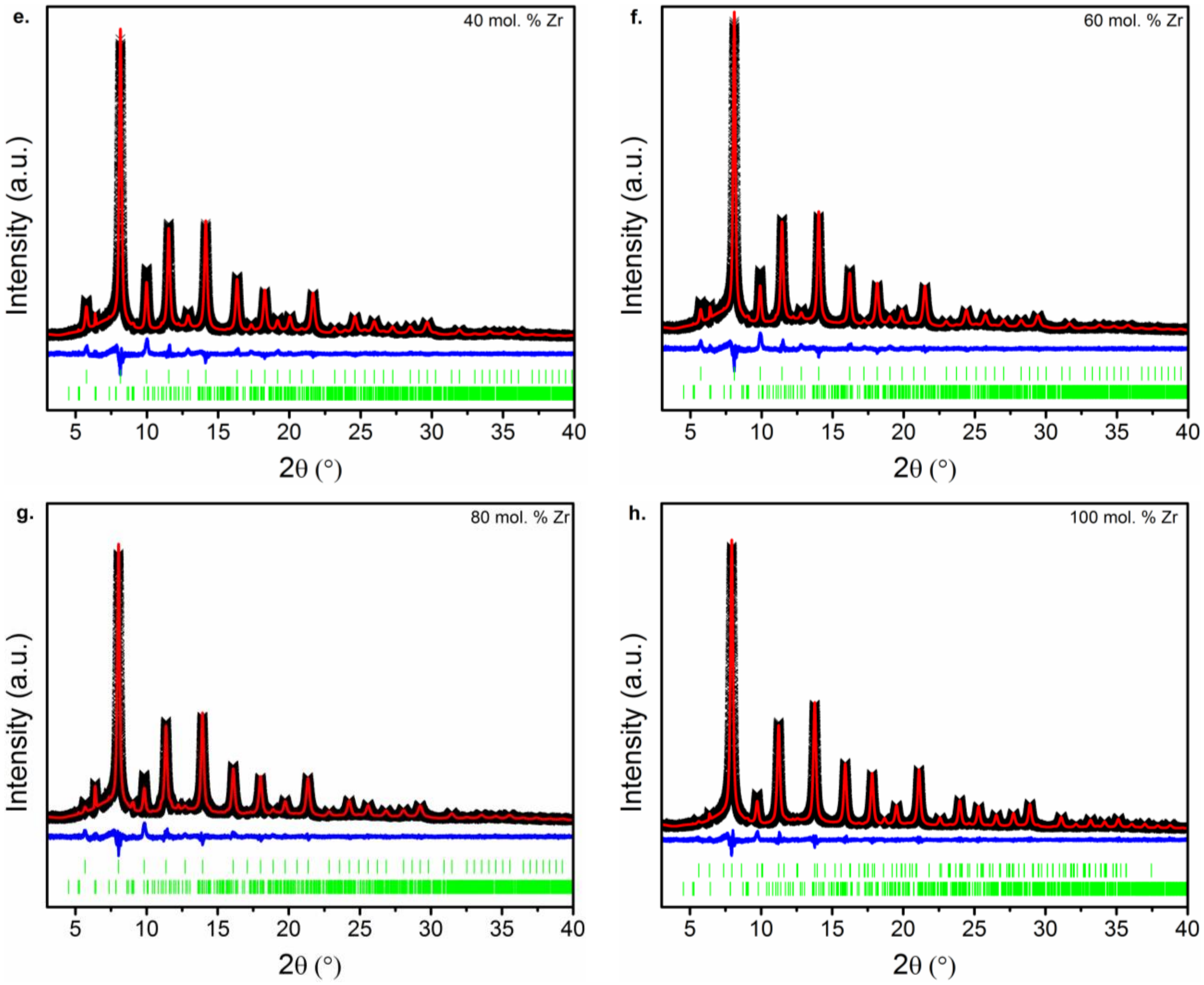

Fig. S2 —*Continued from previous page*. Rietveld analyses of synchrotron X-ray diffraction patterns of $BaZr_xTi_{1-x}O_3$ nanocrystals for the following compositions: (e) $x = 0.4$, (f) $x = 0.6$, (g) $x = 0.8$, and (h) $x = 1$. The experimental (×) and calculated (—) diffraction patterns are shown for each composition, along with the difference curve (—) and the thickmarks (|) corresponding to the two phases refined (upper thickmarks: cubic $BaZr_xTi_{1-x}O_3$; lower thickmarks: orthorhombic $BaCO_3$). $BaCO_3$, which is not observed in the X-ray diffraction patterns of fresh samples, arises from the chemisorption of atmospheric CO_2 upon extended exposure of the nanocrystals to air.

Table S1 Structural Parameters of $BaZr_xTi_{1-x}O_3$ Nanocrystals Obtained via Rietveld Analysis of Synchrotron X-ray Diffraction Data

Zr mol. %	**Structural parameters**					**Refinement residuals**		
	a (Å)[a]	U_{Ba}[b]	$U_{Zr,Ti}$[b]	U_O[b]	$BaCO_3$ wt. %[c]	R_F^2	R_{wp}	χ^2
0	4.038692(31)	0.01026(10)	0.01777(6)	0.00042(17)	13	3.79	4.77	2.03
10	4.059668(32)	0.01273(9)	0.01273(9)	0.01910(14)	9.1	4.49	4.98	1.89
15	4.061279(31)	0.01319(9)	0.01319(9)	0.01978(14)	3.5	4.72	5.42	1.91
20	4.065256(35)	0.01478(11)	0.01478(11)	0.02217(16)	2.0	5.51	6.22	1.86
40	4.105848(40)	0.01461(11)	0.01461(11)	0.02192(11)	1.3	3.93	5.56	2.01
60	4.138891(41)	0.01499(11)	0.01499(11)	0.02248(17)	1.8	4.12	5.50	1.82
80	4.165006(43)	0.01452(11)	0.01452(11)	0.02178(17)	5.0	4.55	5.48	1.54
100	4.212357(24)	0.00957(10)	0.01415(10)	0.00802(23)	1.0	1.97	4.78	1.19

[a] Perovskite phase $BaZr_xTi_{1-x}O_3$. Space group: *Pm*–3*m*. Atomic positions: Ba = (0, 0, 0), Zr,Ti = (½, ½, ½), O = (0, ½, ½). Occupancy factors (not refined): $F_{Ba} = 1$, $F_{Zr} = x$, $F_{Ti} = 1 - x$, $F_O = 3$.

[b] For Zr mol. % ranging from 10 to 80%, the U_{Ba}, $U_{Zr,Ti}$, and U_O were constrained according to: $U_O = 1.5\ U_{Ba} = 1.5\ U_{Zr,Ti}$.

[c] Carbonate phase $BaCO_3$. Space group: *Pmcn*. Refined lattice constants (a, b, c) for each $BaZr_xTi_{1-x}O_3$ composition: (1) $x = 0$: 5.269736(240), 8.979070(449), 6.421566(292); (2) $x = 0.10$: 5.265958(370), 8.975163(691), 6.420260(408); (3) $x = 0.15$: 5.279359(474), 8.958985(930), 6.425164(642); (4) $x = 0.20$: 5.277435(1050), 8.972616(2061), 6.427805(1411); (5) $x = 0.40$: 5.275811(897), 8.981126(1749), 6.427969(1480); (6) $x = 0.60$: 5.281329(1102), 8.976317(2166), 6.427533(1686); (7) $x = 0.80$: 5.276801(744), 8.972539(1402), 6.421544(976); (8) $x = 1.0$: 5.281261(1278), 8.972360(2468), 6.418643(1836). Atomic positions (not refined): Ba = (¼, 0.413197, 0.766602), C = (¼, 0.760100, –0.086400), O(1) = (¼, 0.911900, –0.0946000), O(2) = (0.469400, 0.682100, –0.083900). Isotropic temperature factors (not refined): $U_{Ba} = 0.01$, $U_{C,O} = 0.025$.

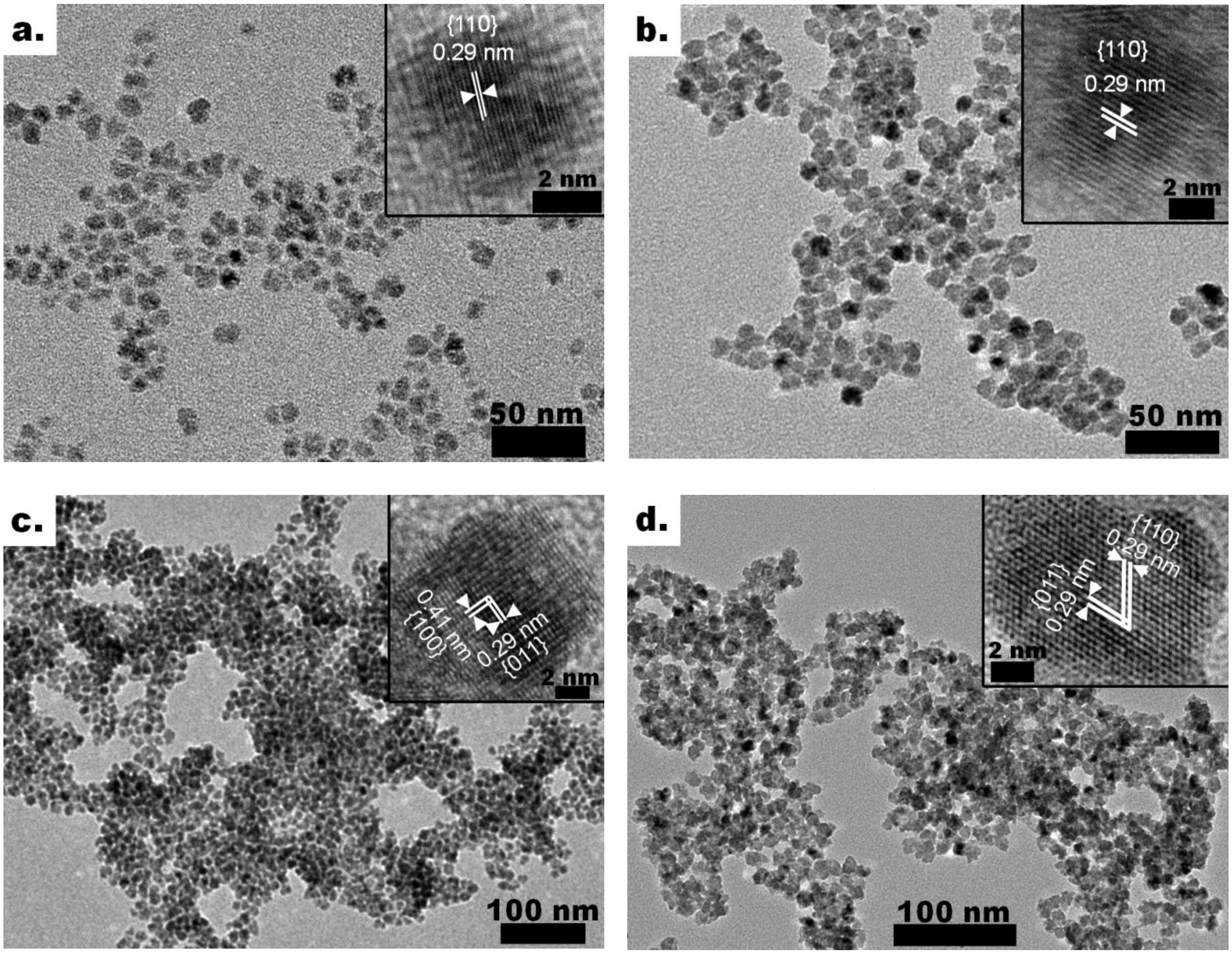

Fig. S3 TEM images of $BaZr_xTi_{1-x}O_3$ nanocrystals for the following compositions: (a) $x = 0$, (b) $x = 0.15$, (c) $x = 0.2$, and (d) $x = 0.4$. For each composition, a high-resolution TEM image of an individual nanocrystal is shown in the inset. —*Continues on the following page*.

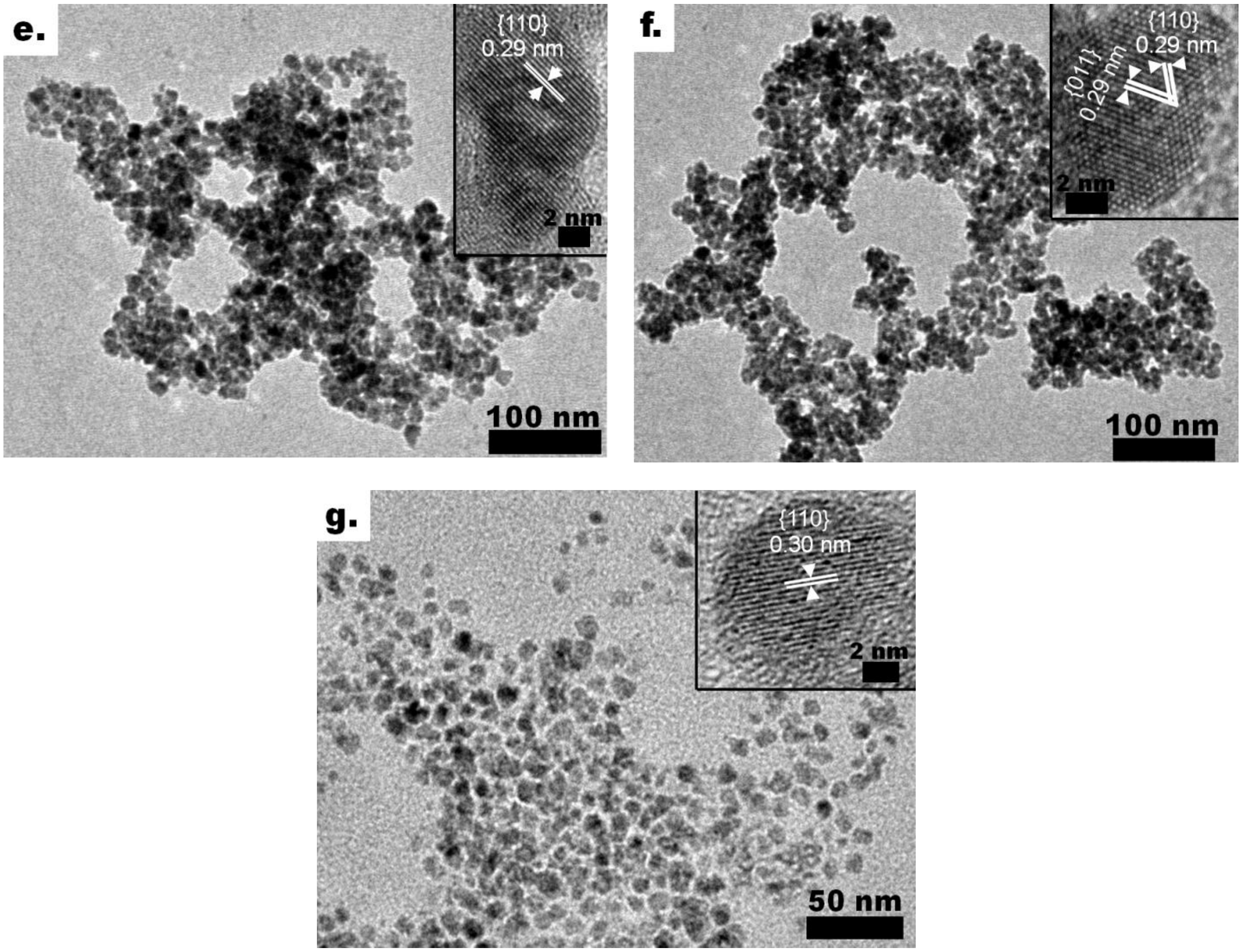

Fig. S3 —*Continued from previous page*. TEM images of $BaZr_xTi_{1-x}O_3$ nanocrystals for the following compositions: (e) $x = 0.6$, (f) $x = 0.8$, and (g) $x = 1$. For each composition, a high-resolution TEM image of an individual nanocrystal is shown in the inset.